

# Preparation and photocatalytic activity of multi-walled carbon nanotubes/Mg-doped ZnO nanohybrids

C.S. CHEN<sup>1,2\*</sup>, X.D. XIE<sup>1</sup>, S.Y. CAO<sup>1</sup>, T.G. LIU<sup>3</sup>, L.W. LIN<sup>2</sup>, X.H. CHEN<sup>3</sup>, Q.C. LIU<sup>1</sup>, J.C. KUANG<sup>1</sup>, Y. XIAO<sup>1</sup>

<sup>1</sup>College of Physics and Electronic Science, Changsha University of Science and Technology, Changsha, 410114, People's Republic of China

<sup>2</sup>State Key Laboratory for Powder Metallurgy, Central South University, Changsha, 410083, People's Republic of China

<sup>3</sup>College of Physics and Microelectronics Science, Hunan University, Changsha, 410082, People's Republic of China

Multi-walled carbon nanotubes/Mg-doped ZnO (MWNTs/Zn<sub>1-x</sub>Mg<sub>x</sub>O) nanohybrids were prepared by co-precipitation method, and their photocatalytic activity for methyl orange (MO) was studied. Experimental results showed that Mg-doped ZnO nanoparticles were successfully deposited on the surface of MWNTs under annealing at 450 °C and 550 °C. The resultant MWNTs/Zn<sub>0.9</sub>Mg<sub>0.1</sub>O nanohybrids had better photocatalytic activity for degradation of methyl orange than pure ZnO: the rates of MO photodegradation were 100 % and 30 % for 1 h, respectively. The enhancement in the photocatalytic activity was attributed to the excellent electronic properties of MWNTs and Mg-doping.

Keywords: *carbon nanotube; Mg-doped ZnO; nanohybrids; photocatalytic activity*

© Wroclaw University of Technology.

## 1. Introduction

Zinc oxide (ZnO) has attracted great interests due to its high optical activity and stability, wide band gap of 3.37 eV, large exciton binding energy (60 meV) at room temperature, low cost and environmental friendliness [1–3]. Such fascinating properties render ZnO as a promising candidate for the photocatalysis and degradation of various organic pollutants. Unfortunately, there are two major drawbacks for photocatalytic practical application of ZnO. One is that it does not absorb visible light due to its high band gap energy, and the other is that it possesses lower photocatalytic efficiency because of the recombination of photogenerated electron-hole pairs.

In order to utilize solar radiations more effectively, metal and anionic doping were employed previously for improving the photocatalytic activity of ZnO under sunlight irradiation. Among various dopants, Mg<sup>2+</sup> has a ionic radius of 0.57 Å,

which is very close to the ionic radius of Zn<sup>2+</sup> (0.60 Å), therefore, Mg ions have a large solubility in ZnO and ability to replace Zn, but Mg does not give rise to significant changes in the lattice constants [4]. Mg doping can create localized impurity levels by replacing the Zn site of ZnO lattice, or inserting into the crystal lattice of ZnO, resulting in creating localized impurity levels and creating many intermediate energy gaps in ZnO crystal [5–9]. Therefore, Mg-doping can improve the photocatalytic activity of ZnO nanostructures significantly [10].

Carbon nanotubes (CNTs) are considered to be an ideal excellent supporting material for catalyst nanoparticles owing to their unique internal structure, high surface area, extremely high mechanical strength, remarkable chemical stability, and outstanding electronic conductivity [11–13]. As a catalyst carrier, CNTs can not only act as photosensitizers for catalysts [14] but also hinder the recombination of electrons and holes [15]. More importantly, CNTs have a large surface area, and can act as a dispersing agent that prevents catalyst

\*E-mail: jxccc1934@gmail.com

nanoparticles from agglomerating [16], which results in providing higher active surface area. Thus, CNTs are widely employed to enhance the photocatalytic activity of ZnO nanoparticles [17–21].

Although there has been a large progress in the synthesis of CNTs/ZnO composite, CNTs often exist in the form of highly tangled ropes, and are poorly dispersible. Furthermore, it is very difficult to control homogeneity and the quality of ZnO nanoparticles coating the surface of CNTs. In addition, further improvement in the absorption of visible light and increasing optical quantum efficiency are essential prerequisites for boosting photocatalytic activity of CNTs/ZnO composite. In this paper, a facile and efficient approach of treating MWNTs has been developed to support ZnO nanoparticles on MWNTs, and the band-gap of ZnO nanoparticles has been modulated by Mg doping. MWNTs were treated by sodium hydroxide and then a mixture of acids. Subsequently, the surface of MWNTs was decorated with Mg-doped ZnO nanoparticles and the photocatalytic activity of MWNTs/Mg-doped ZnO nanohybrids was studied.

## 2. Experimental

### 2.1. Preparation and treatment of MWNTs

MWNTs used in the experiment were prepared by the chemical catalytic vapor decomposition process (CVD) [22]. The inner diameters, outer diameters and length of the prepared MWNTs were measured to be 10 nm, 20 nm and 1  $\mu\text{m}$ , respectively. In a typical treatment, 5g as-prepared MWNTs were dispersed in 500 mL sodium hydroxide (2 mol/L) and refluxed at boiling point for 2 h under stirring. After rinsing with deionized water until the pH value of solution closed to neutral, the NaOH-treated MWNTs were dried at 80 °C. In order to remove impurities, these NaOH-treated MWNTs were further oxidized by immersing in a 3:1 mixture of concentrated  $\text{H}_2\text{SO}_4$  and  $\text{HNO}_3$  and refluxing for 2 h at boiling point, subsequently dispersing in 500 mL HCl solution (2 mol/L) and refluxing for another 2 h at the same temperature. Finally, the

MWNTs were dried at 80 °C after being filtered and washed with deionized water. The details of treating MWNTs have been described in our previous report [23].

### 2.2. Preparation of MWNTs/ $\text{Zn}_{1-x}\text{Mg}_x\text{O}$ hybrids

MWNTs/ $\text{Zn}_{1-x}\text{Mg}_x\text{O}$  nanohybrids were prepared as follows: Firstly, 0.05 g of the MWNTs, treated according to previously described procedure, were added into 100 mL anhydrous ethanol and sonicated for about 15 min, and then 2.2g  $\text{Zn}(\text{CH}_3\text{COO})_2 \cdot 2\text{H}_2\text{O}$  and appropriate  $\text{Mg}(\text{CH}_3\text{COO})_2 \cdot 2\text{H}_2\text{O}$  (the molar ratios of Mg to Zn were 5:95, 1:9, 0.2:0.8, and 0.3:0.7, respectively) were added into the MWNTs dispersed in anhydrous ethanol. Subsequently, an appropriate amount of oxalic acid (the molar ratio of metal ion to oxalic acid was 1.1) was dissolved in 100 mL anhydrous ethanol, and then slowly dropped into the mixture solution of zinc acetate and magnesium acetate, while stirring at 60 °C, and a sol was produced. Thirdly, the sol was maintained at 80 °C for 48 h to form the precursor. Finally, the resultant precursor was annealed in nitrogen from room temperature to setting temperature at a rate of 5 °C $\cdot\text{min}^{-1}$ , and then held at the setting temperature for 2 h. The setting temperature was 450 °C, 550 °C, 650 °C, and 700 °C, respectively. For comparison, the ZnO nanoparticles and MWNTs/ZnO nanohybrids annealed at 650 °C were prepared under the same conditions.

### 2.3. Characterization

Infrared spectroscopy was performed using a 300E Jasco spectrophotometer at room temperature. X-ray diffraction (XRD) measurements were performed using Philips PW 1710 diffractometer with  $\text{CuK}\alpha_1$  radiation. The nature of chemical state of MWNTs nanohybrids was analysed using X-ray photoelectron spectroscopy (XPS) with a Kratos AXIS-165 spectrometer. Scanning electron microscopy (SEM) observations and the energy dispersive X-ray spectroscopy (EDS) were carried out with an S-4800 field emission scanning electron microscope. Transmission electron

microscopy (TEM) analyses were conducted on a JEM-3010 transmission electron microscope. Fluorescence spectra measurements were performed for anhydrous ethanol on a Hitachi F4500 fluorescence spectrophotometer at room temperature.

Methyl orange (MO) was used as a model dye to evaluate the photocatalytic activity of MWNTs/Mg-doped ZnO hybrids. In a typical experiment, 50 mg catalyst was dispersed in 200 mL of 20g/L MO aqueous solution. The above reaction mixture was magnetically stirred for 30 min in dark, and then the photoreactions were conducted at room temperature under a high pressure Osram Ultra-Vitalux lamp (100 W, wave length 365 nm) positioned horizontally above the liquid surface (the lamp was placed at about 40 cm above the solution surface). The methyl orange aqueous solution was magnetically stirred throughout the photocatalytic experiment to ensure the full suspension of particles. The experiments were conducted for 60 min with 3 mL sample aliquots extracted every 15 min and subsequently centrifuged at 4000 rpm for 10 min. The decomposition of methyl orange was monitored by measuring the absorbance of the supernatant at 464 nm using TU-2550 spectrophotometer. The degradation ratio was calculated with  $(C/C_0)$ , where  $C_0$  is the initial concentration and  $C$  is the concentration of MO in solution at different time.

### 3. Results and discussion

#### 3.1. Infrared spectrum analysis

Fig. 1 shows the infrared spectra of different MWNTs. It can be seen that no peaks are observed in the spectrum of pristine MWNTs (curve a in Fig. 1). However, when the MWNTs were treated, many groups were introduced onto their surfaces. There were carbonyl groups revealed at about  $1705\text{ cm}^{-1}$ , oxygen-hydrogen bonds and C=C bonds revealed at about  $3427\text{ cm}^{-1}$  and  $1568\text{ cm}^{-1}$ , respectively, as shown in curve b and curve c of Fig. 1. It is worth noting that NaOH treatment could enhance the intensity of oxygen-hydrogen bonds significantly, which indicates that the surface activity of MWNTs has been further improved.

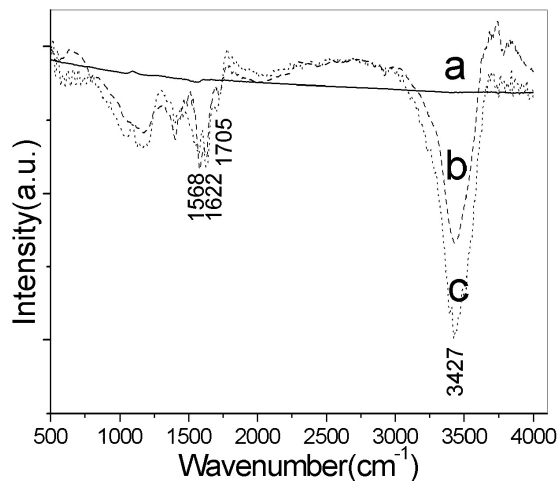


Fig. 1. Infrared spectrum of different MWNTs: (a) as-prepared, (b) treated by mixture acid, and (c) treated by NaOH and mixture acid.

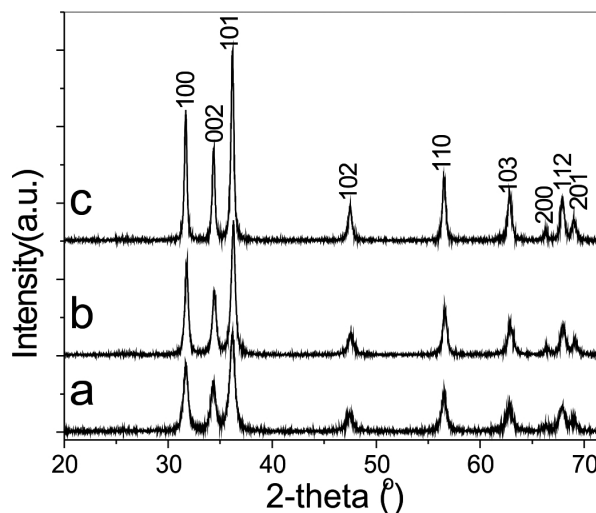


Fig. 2. XRD patterns of the MWNTs/ $\text{Zn}_{0.9}\text{Mg}_{0.1}\text{O}$  nanohybrid annealed at different temperatures: (a)  $450\text{ }^\circ\text{C}$ , (b)  $550\text{ }^\circ\text{C}$ , (c)  $650\text{ }^\circ\text{C}$ .

#### 3.2. XRD analysis

Fig. 2 displays the XRD patterns of MWNTs/ $\text{Zn}_{0.9}\text{Mg}_{0.1}\text{O}$  nanohybrid subjected to heat treatment at different temperatures. It has been found that all samples exhibit the diffraction peaks of ZnO corresponding to (100), (002), (101), (102), (110), (103), (200), (112) and (201) planes, respectively. All diffraction peaks of the samples are in good agreement with those of the

hexagonal wurtzite structure of ZnO (JCPDS Card No. 36-1451). Comparison of the three curves shows that the diffraction peaks become sharper and narrower with increasing temperature of heat treatment, which indicates that the crystallite size increases along with the rise of temperature of heat treatment. Furthermore, no traces of magnesium metal, oxides, or any binary zinc magnesium phases are observed in the XRD pattern. This result illustrates that doping with Mg may replace the Zn site of ZnO lattice, or insert into the crystal lattice of ZnO.

### 3.3. SEM studies

SEM images of MWNTs/ $Zn_{0.9}Mg_{0.1}O$  nanohybrids annealed at different temperatures are shown in Fig. 3. As shown in Fig. 3a, it can be found that MWNTs/ $Zn_{0.9}Mg_{0.1}O$  nanohybrids annealed at 450 °C are composed of nanowires, and the nanoparticle size is about 10 nm. However, when the temperature of heat treatment was increased to 550 °C, the MWNTs/ $Zn_{0.9}Mg_{0.1}O$  nanohybrids were still composed of nanowires but the nanoparticle size changed into about 20 nm (Fig. 3b). Further increasing of the treatment temperature up to 650 °C, resulted in the MWNTs/ $Zn_{0.9}Mg_{0.1}O$  nanohybrids composed of MWNTs and nanoparticles with the size of about 60 nm (Fig. 3c). Fig. 3d displays the SEM images of  $Zn_{0.9}Mg_{0.1}O$  nanohybrids annealed at 650 °C. It is clear that the nanoparticles reunited to large aggregates. This result implies that MWNTs can improve the dispersion of nanoparticles.

In order to analyse the elements present in the nanoparticles on the surface of MWNTs, EDS was carried out, and the ratio of each element is shown in Table 1. It reveals the presence of Zn, O, Mg, and C, which confirms that the nanoparticles on the surface of MWNTs are Mg-doped ZnO nanoparticles. From Table 1, we can conclude that the ratio of Zn to Mg increased as the annealed temperature increased, however, the ratio of O to metal element decreased. When the annealing temperature was 450 °C, the ratios of Zn to Mg and O to metal were about 7.12 and 1.44, respectively. After increasing the annealing temperature to 650 °C,

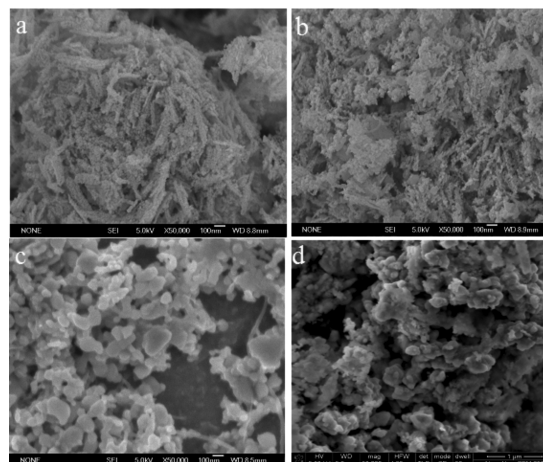


Fig. 3. SEM images of MWNTs/ $Zn_{0.9}Mg_{0.1}O$  nanohybrids annealed at 450 °C (a), 550 °C (b), and 650 °C (c); SEM images of  $Zn_{0.9}Mg_{0.1}O$  nanohybrids annealed at 650 °C (d).

their ratios changed to 9.2 and 0.88, respectively. These results show that the annealing temperature affects the oxygen vacancies and zinc vacancies of ZnO crystal.

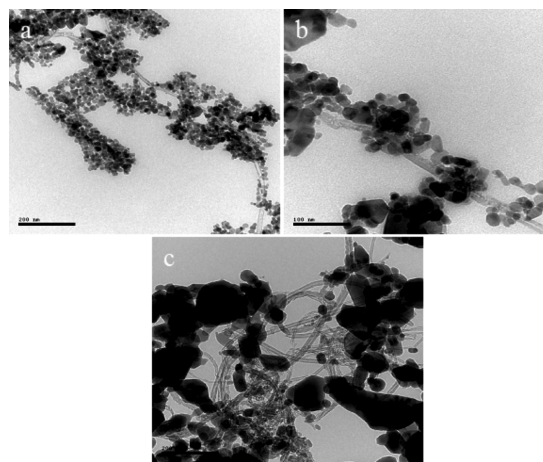


Fig. 4. TEM images of MWNTs/ $Zn_{0.9}Mg_{0.1}O$  nanohybrids annealed at different temperatures: (a) 450 °C, (b) 550 °C, and (c) 650 °C.

### 3.4. TEM studies

TEM studies further confirmed the successful attachment of Mg-doped ZnO nanoparticles to the walls of MWNTs, as shown in Fig. 4. Fig. 4a shows the TEM image of MWNTs/ $Zn_{0.9}Mg_{0.1}O$

Table 1. the EDS of different samples.

Element	C (at.%)	O (at.%)	Zn (at.%)	Mg (at.%)
MWNTs/Zn <sub>0.9</sub> Mg <sub>0.1</sub> O nanohybrids annealed at 450 °C	16.91	49.06	29.84	4.19
MWNTs/Zn <sub>0.9</sub> Mg <sub>0.1</sub> O nanohybrids annealed at 550 °C	13.43	47.68	34.47	4.42
MWNTs/Zn <sub>0.9</sub> Mg <sub>0.1</sub> O nanohybrids annealed at 650 °C	10.82	41.88	42.68	4.63

nanohybrids annealed at 450 °C. It is evident that the surface of the MWNTs is decorated by a large number of nanoparticles, and the size distribution of the ZnO nanoparticles is narrow, with an average particle size of about 10 nm. Fig. 4b reveals the TEM image of MWNTs/Zn<sub>0.9</sub>Mg<sub>0.1</sub>O nanohybrids annealed at 550 °C. It can be observed that the MWNTs are continuously coated by nanoparticles with the size of about 20 nm. When the temperature of heat treatment reached 650 °C, not only the particle size of nanoparticles further increased, but also the discontinuity in the coating became apparent, as shown in Fig. 4c. These results illustrate that the size of nanoparticles on the surface of MWNTs increased with increasing the annealing temperature.

### 3.5. XPS analysis

The composition and chemical states of the MWNTs/Zn<sub>0.9</sub>Mg<sub>0.1</sub>O nanohybrid were analyzed using XPS spectra. Fig. 5 displays the O 1s, Zn 2p, and Mg 1s XPS spectra of MWNTs/ZnO and MWNTs/Zn<sub>0.9</sub>Mg<sub>0.1</sub>O nanohybrid annealed at 650 °C. It is demonstrated in Fig. 5a that the O 1s core-level spectrum of nanohybrid shows three O 1s peaks and a O 1s peak band. The O 1s peak positioned at the lower binding energy of 529.8 eV has been assigned to O<sup>2-</sup> ions in the Zn–O binding of wurtzite structure of ZnO. The two peaks located at 530.2 and 530.8 eV have been ascribed to the added contribution from Zn–O–Mg and Mg–O bonds, respectively. The band located at 532.0 eV is attributed to the Zn–OH bonding, which is in agreement with the previous report of Mg-doped ZnO thin film [24]. From Fig. 5b, it can be seen that the Zn 2p core-level of MWNTs/ZnO nanohybrid has two fitting peaks located at about 1044.30 and 1021.30 eV attributed to Zn 2p<sub>1/2</sub> and

Zn 2p<sub>3/2</sub>, respectively. Similarly, the Zn 2p core-level of MWNTs/Zn<sub>0.9</sub>Mg<sub>0.1</sub>O nanohybrids have two fitting peaks shifted towards the higher binding energy. Those two fitting peaks are located at about 1044.70 and 1021.70 eV, respectively. Moreover, it can be seen that the binding energy difference between the Zn 2p<sub>1/2</sub> and Zn 2p<sub>3/2</sub> is 23 eV for all MWNTs nanohybrids. These results indicate that the chemical valence of Zn at the surface of MWNTs nanohybrids is +2 oxidation state [25]. The Mg 1s peak is shown in Fig. 5c. Mg 1s peak at 1303.98 eV belongs to the Mg–O bonding in ZnO [26]. XPS measurements combined with XRD results demonstrated that the Mg successfully replaced the Zn site of ZnO lattice.

### 3.6. Decoration mechanism

We presumed that the MWNTs-supported Mg-doped ZnO nanoparticles were attributed to enhance the surface activity of MWNTs by the treatment with NaOH solution and mixture acid. After MWNTs were treated by NaOH and mixture acid, more defects were produced on the walls of MWNTs, which was also favorable for the deposition of nanoparticles on the surface of MWNTs. Fig. 6 displays the HRTEM images of different MWNTs. It can be seen that there is an amorphous layer on the outer layer of pristine MWNTs, as shown in Fig. 6a. After treating MWNTs with NaOH and mixture acid, not only the amorphous layer was eliminated completely, but also some defects on the outer wall of MWNTs have revealed (Fig. 6b). This result illustrates that the carbon atoms of MWNTs walls were etched by NaOH solution and mixture acid.

In addition, the decorating nanoparticles on the surface of MWNTs can be attributed to the oxygen functional groups, such as carboxyl

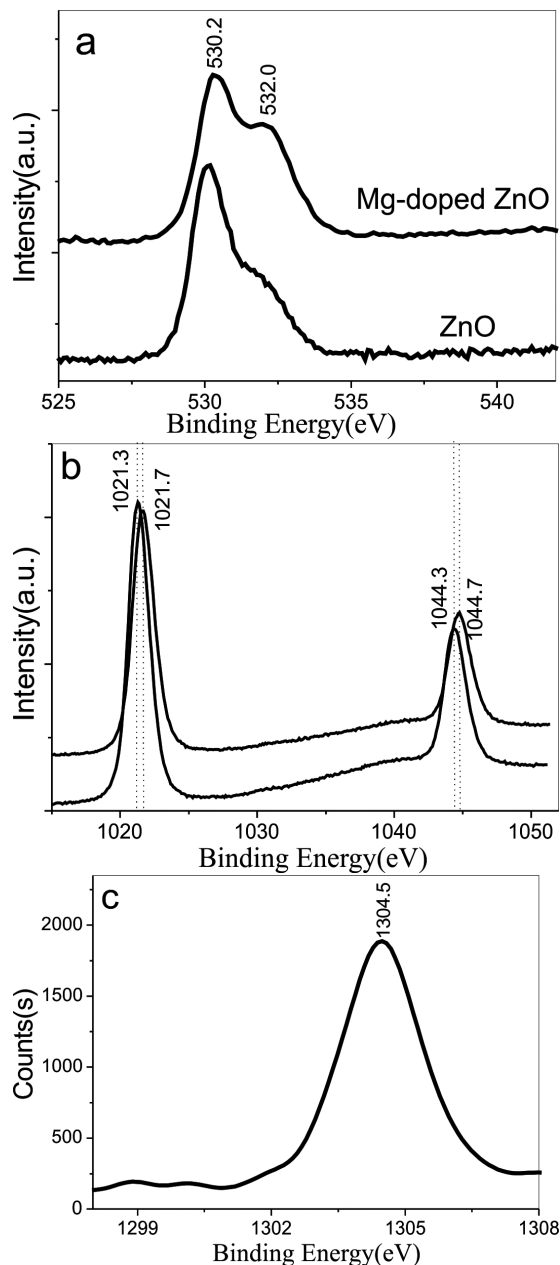


Fig. 5. XPS spectrum of MWNTs/ZnO nanohybrid and MWNTs/Zn<sub>0.9</sub>Mg<sub>0.1</sub>O nanohybrid annealed at 650 °C: (a) O 1s, (b) Zn 2p, and (c) Mg 1s.

groups and oxygen-hydrogen groups, facilitating the interaction between MWNTs and oxalate precursor. These oxygen functional groups on the walls of MWNTs can improve the chemical activity and dispersion of MWNTs. Furthermore, these carboxyl groups can form carboxyl group with negative charge in solution, and easily attract

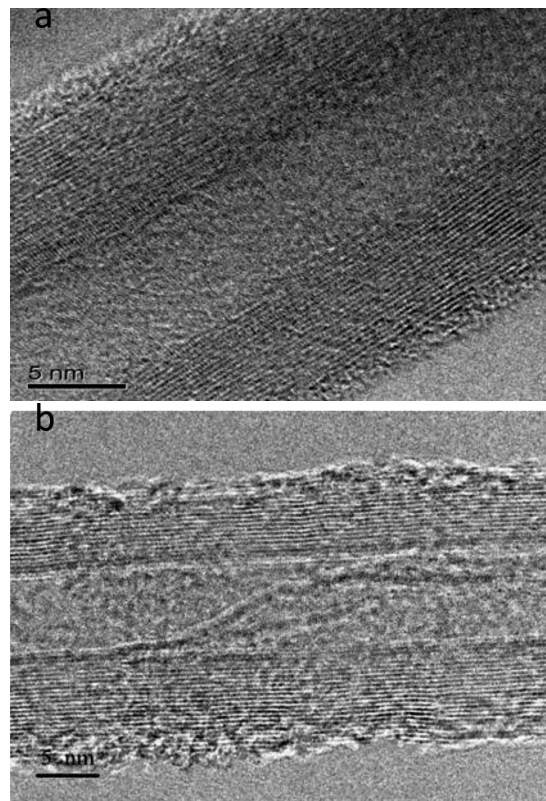
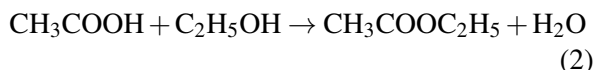
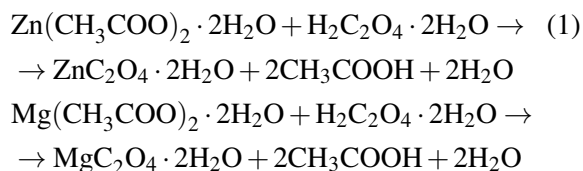


Fig. 6. TEM images of different MWNTs: (a) as-prepared and (b) treated by NaOH.

positively charged metal ions through electrostatic interactions. When the H<sub>2</sub>C<sub>2</sub>O<sub>4</sub> and C<sub>2</sub>H<sub>5</sub>OH were added, the Zn<sup>2+</sup> and Mg<sup>2+</sup> easily formed ZnC<sub>2</sub>O<sub>4</sub> and MgC<sub>2</sub>O<sub>4</sub>, which underwent the combination reaction as described in equation 1. The CH<sub>3</sub>COOH can react with C<sub>2</sub>H<sub>5</sub>OH by esterification (equation 2), accelerated towards the right (equation 1) and help in the formation of ZnC<sub>2</sub>O<sub>4</sub> and MgC<sub>2</sub>O<sub>4</sub>. The reaction of combination (equation 1) and esterification (equation 2) happened almost at the same time. Ultimately, all the Zn<sup>2+</sup> and Mg<sup>2+</sup> were turned into oxalate precursor. Every metal ion was bonded by C<sub>2</sub>O<sub>4</sub><sup>2-</sup> ions to form a planar molecule in the complexes. There were two coordinated H<sub>2</sub>O molecules at each side of the molecular plane and two molecular planes were connected by the H<sub>2</sub>O molecule (shown in Fig. 7). Hence, MWNTs can uniformly support oxalate precursor by hydrogen bond in ethanol solution. Finally, when the MWNTs/oxalate

precursor was annealed at low temperature, the oxalate precursor released CO and CO<sub>2</sub> gas, simultaneously producing ZnO and MgO, resulting in formation of Mg-doped ZnO nanoparticles accumulating on the surface of MWNTs. The chemical reaction was displayed in equation 3. When the heating time was prolonged, the small oxide nanoparticles nucleated on MWNTs and grew into large oxide crystallites. Therefore, the MWNTs could be decorated by nanoparticles uniformly. However, when the MWNTs/oxalate precursor was annealed at high temperature, the particle size on MWNTs further increased, resulting in MWNTs protruding from the nanoparticles.



### 3.7. Photocatalytic studies

Methyl orange (MO) is a common organic dye with orange color, which is widely used to evaluate the photocatalytic activity of photocatalysts [27]. Fig. 8 depicts the photocatalytic photodegradation efficiency of different samples for MO. The photocatalysts loading content is 0.25 g/L. It is found that the blank test (without any sample) has shown only a small amount of MO degradation. The photoactivity of the MWNTs/Zn<sub>0.9</sub>Mg<sub>0.1</sub>O samples has been enhanced with increasing annealing temperature from 450 °C to 650 °C. When the annealing temperature increased beyond 650 °C, the photocatalytic performance decreased. These results indicate that the optimum annealing temperature is 650 °C. This is because the nanoparticles on MWNTs became larger under high annealing temperature, and MWNTs were devoid of nanoparticles, resulting in weakening the interaction of MWNTs and nanoparticles.

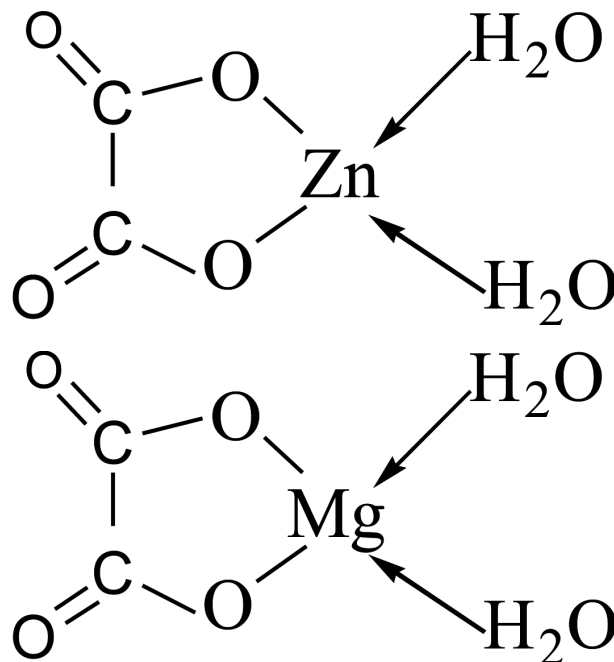


Fig. 7. The structures of ZnC<sub>2</sub>O<sub>4</sub>·2H<sub>2</sub>O and MgC<sub>2</sub>O<sub>4</sub>·2H<sub>2</sub>O precursors.

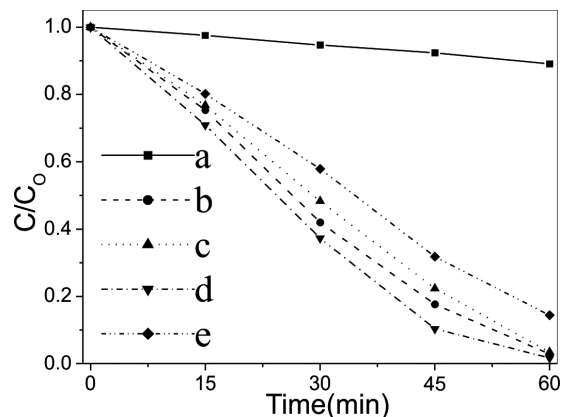


Fig. 8. Photocatalytic performance of MWNTs/Zn<sub>0.9</sub>Mg<sub>0.1</sub>O nano hybrids at different annealing temperatures: (a) blank, (b) 450 °C, (c) 550 °C, (d) 650 °C, (e) 700 °C.

To study the effect of Mg-doping content on the photocatalytic activity of MWNTs/Zn<sub>1-x</sub>Mg<sub>x</sub>O nano hybrids, we tested the photocatalytic activity of MWNTs/Zn<sub>1-x</sub>Mg<sub>x</sub>O nano hybrids annealed at 650 °C, and the result is shown in Fig. 9. Obviously, the amount of MO degraded by the pure ZnO sample was about 34 % after 60 min, and the

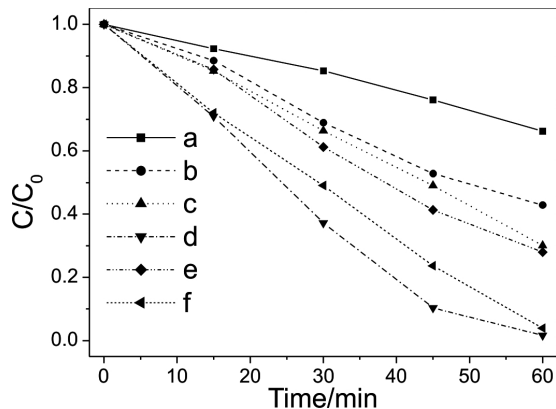


Fig. 9. Photocatalytic performance of MWNTs/ $Zn_{1-x}Mg_xO$  nano hybrids annealed at 650 °C: (a) ZnO, (b) MWNTs/ZnO nano hybrids, (c) MWNTs/ $Zn_{0.95}Mg_{0.05}O$  nano hybrids, (d) MWNTs/ $Zn_{0.9}Mg_{0.1}O$  nano hybrids, (e) MWNTs/ $Zn_{0.8}Mg_{0.2}O$  nano hybrids, (f) MWNTs/ $Zn_{0.7}Mg_{0.3}O$  nano hybrids.

MWNTs/ZnO hybrid sample exhibited higher photocatalytic degradation efficiency than pure ZnO sample, which came up to about 58 %. It is worth to note that the photocatalytic degradation efficiency of all MWNTs/ $Zn_{1-x}Mg_xO$  hybrids was higher than that of the MWNTs/ZnO nano hybrids sample, in which the amount of degraded MO was about 100 % within 60 min, implying that the photocatalytic ability of MWNTs/ZnO hybrids for MO was improved by Mg-doping. Also, the photocatalytic activity of the samples was enhanced with increasing Mg concentration from 0 to 0.1. As the Mg content increased beyond 0.1, the photocatalytic activity decreased. These results indicated that there was an optimum ratio between Mg element and Zn element for improving the photocatalytic activity, and the optimum mass ratio of Mg to Zn was 1:9.

### 3.8. Fluorescence analysis

Fig. 10 shows the room-temperature fluorescence spectra of different samples, obtained at the wavelength of excitation of 320 nm. There is a UV peak at about 354 nm on the spectrum of MWNTs (curve a in Fig. 10a), which comes from the trapping of excitation energy at defect sites of MWNTs and the increasing of energy gap between the lowest empty orbital and the highest occupied orbital

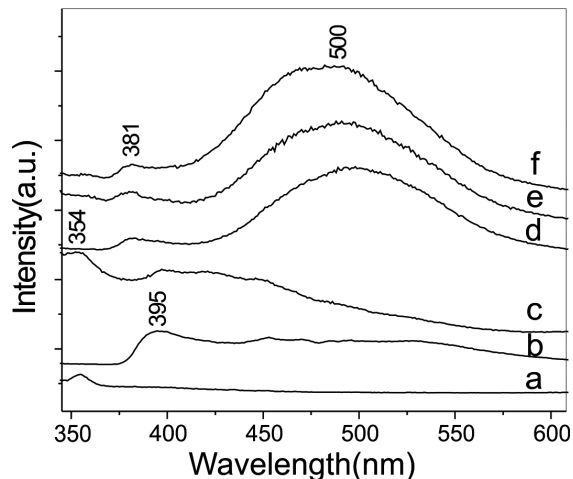


Fig. 10. Fluorescence spectra of different samples: (a) MWNTs, (b) pure ZnO, (c) MWNTs/ZnO hybrid annealed at 450 °C, (d) MWNTs/ $Zn_{0.9}Mg_{0.1}O$  hybrid annealed at 450 °C, (e) MWNTs/ $Zn_{0.9}Mg_{0.1}O$  hybrid annealed at 550 °C, (f) MWNTs/ $Zn_{0.9}Mg_{0.1}O$  hybrid annealed at 650 °C.

of the modified MWNTs [28]. Then, the fluorescence spectrum of ZnO nanoparticle (curve b in Fig. 10) shows the UV emission peak at 395 nm, which originates from the exciton recombination corresponding to the near-band edge (NBE) exciton emission of the wide band gap ZnO, namely, the free excitons recombination through exciton-exciton collision process. In the fluorescence spectrum of MWNTs/ZnO hybrid annealed at 450 °C, there is a UV peak at about 354 nm besides the intrinsic peak of ZnO at 395 nm, as shown in curve c in Fig. 10. However, the fluorescence spectra of all MWNTs/ $Zn_{0.9}Mg_{0.1}O$  hybrids (shown in curves d, e and f in Fig. 10) include an UV emission peak at about 381 nm and a green emission band center at about 500 nm, which can be attributed to the singly ionized oxygen vacancy in the ZnO nanostructures [29].

The blue-shift of ultraviolet emission peak is attributed to Mg replacing the zinc site of ZnO lattice, which results in extending the band gap of ZnO towards the deep UV region in the ZnO [30]. Moreover, the blue-shift of ultraviolet emission peak may originate from Moss-Burstein effect, which describes the upward movement of Fermi

level with Mg doping [31]. Because the sizes of the samples are much larger than the exciton Bohr radius of 1.8 nm, we think that the blue-shift of green emission peak does not originate from quantum confinement effects, but rather is attributed to Mg replacing the zinc site of ZnO lattice. When magnesium replaces the zinc site of ZnO lattice, oxygen vacancies and electron concentration increase. Generally, as the Fermi level of intrinsic ZnO is inside the conduction band, many electrons generated by Mg dopant locate at a higher Fermi level. Therefore, the radiative recombination of excitons causes a blueshift [32]. Furthermore, the substitution of Zn by Mg makes the polarization of its neighboring  $O^{2-}$  ion decrease, causing the defect band to move towards the ultraviolet [33]. Meanwhile, the Mg-doping can shift the conduction-band and valence-band levels to the same degree in relation to the  $V_O$  level [34].

In addition, with increasing doping of Mg in ZnO, we found that the ultraviolet emission peak of ZnO shifted from 395 nm to 381 nm, and the intensity of the green emission peak was greater than that of ultraviolet emission peak. Furthermore, the green emission peak shifted to blue region with increasing the Mg-doping content in ZnO. The blue-shift of ultraviolet emission peak is attributed to Mg replacing the site of ZnO lattice, resulting in extending the band gap of ZnO towards the deep UV region of the ZnO. The enhancement of green emission peak can be explained that when magnesium replaces the zinc site of ZnO lattice or inserts into the Zn interstitial, the lattice of ZnO is distorted and forms oxygen vacancies and zinc vacancies, resulting in improving the intensity of green emission peak significantly [35]. These results indicate that some Mg cations in the hybrids are incorporated in the Zn cation sites, and others Mg cations are inserted into the Zn interstitial.

### 3.9. Photocatalytic mechanism

As we discussed above, it has been concluded that the enhancement in photocatalytic activity is attributed to the outstanding electrical property of MWNTs and the defects in the ZnO crystals caused by Mg-doping. When magnesium replaces the zinc

site of ZnO lattice or inserts into the Zn interstitial, the lattice of ZnO is distorted and forms oxygen vacancies and zinc vacancies, resulting in creating intermediate energy gap in ZnO crystal. The intermediate energy gap can promote the absorption of photons and create electron-hole pairs. Under UV-light irradiation, the electrons ( $e^-$ ) in the valence band (VB) of ZnO are excited to the conduction band (CB), leaving holes ( $h^+$ ) in the VB. MWNTs have a large electron-storage capacity (one electron for every 32 carbon atoms), and it is easy to capture photogenerated electrons ( $e^-$ ) from the CB of ZnO, hindering the recombination of electron-hole pairs. The photogenerated holes ( $h^+$ ) can migrate to the ZnO surface easily, and directly oxidize the adsorbed MO into  $CO_2$  and  $H_2O$ . Simultaneously, more photogenerated holes can react with adsorbed water to form hydroxyl radical ( $\cdot OH$ ), which is available to promote the decomposition of MO. Furthermore, the oxygen adsorbed on the surface of ZnO may accept  $e^-$  and form  $\cdot O_2^-$ , which also leads to the formation of  $\cdot OH$ , resulting in degrading the MO. The process of electron transport in MWNTs/ZnO hybrids and photocatalytic degradation are shown in Fig. 11.

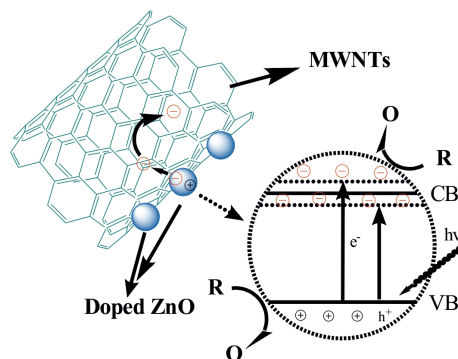


Fig. 11. The complete scheme of electron transfer in MWNTs/ZnO hybrids and photocatalytic degradation.

## 4. Conclusion

In summary, Mg-doped ZnO nanoparticles were successfully decorated onto the surface of MWNTs through the co-precipitation method. It is worth to note that the resultant MWNTs/ $Zn_{0.9}Mg_{0.1}O$  hybrids have very strong

green emission, and are proved to be highly active for photocatalytic degradation of methyl orange (MO). This is because MWNTs can act as photosensitizers for ZnO nanoparticles and hinder the recombination of electron-hole pairs. Moreover, incorporating Mg into ZnO can create an intermediate energy gap between the valence and conduction band of ZnO, and promote the absorption of photons, resulting in creating more electron-hole pairs. Accordingly, the synthetic products have a potential application in fields of photocatalysis, sewage treatment and environmental protection.

### Acknowledgements

C.S. Chen thanks the National Science Foundation of China (Nos. 21276028, 51154001, 51302021 and 11004018), Hunan Provincial Natural Science Foundation of China (Nos.09JJ3095 and 14JJ2077), National (Ministry of Land and Resources) Public Welfare Scientific Research (No.201011031), the Construct Program of the Key Discipline in Hunan Province, and Aid Program for Science and Technology Innovative Research Team in Higher Educational Institutions of Hunan Province for financial supports.

### References

- [1] HUANG M.H., MAO S., FEICK H., YAN H., WU Y., KIND H., WEBBER E., RUSSO R., YANG P., *Science*, 292 (2001), 1897.
- [2] RENSMO H., KEIS K., LINDSTROM H., SODERGREN S., SOLBRAND A., HAGFELDT A., LINDQUIST S.E., WANG L.N., MUHAMMED M., *J. Phys. Chem. B*, 101 (1997), 2598.
- [3] AL-HILI S.M., AL-MOFARJI R.T., WILLANDER M., *Appl. Phys. Lett.*, 89 (2006), 173119.
- [4] SHANNON R.D., *Acta Crystallogr. A*, 32 (1976), 751.
- [5] LI H., ZHANG Y.Z., PAN X.J., ZHANG H.L., WANG T., XIE E., *J. Nanopart. Res.*, 11 (2009), 917.
- [6] SAHAL M., MARI B., MOLLAR M., MANJON F.J., *Phys. Status Solidi C*, 79 (2010), 2306.
- [7] WANG Y.S., THOMAS P.J., O'BRIEN P., *J. Phys. Chem. B*, 43 (2006), 21412.
- [8] YADAV M.K., GHOSH M., BISWAS R., RAYCHAUDHURI A.K., MOOKERJEE A., *Phys. Rev. B*, 76 (2007), 195450.
- [9] FUJIHARA S., OGAWA Y., KASAI A., *Chem. Mater.*, 16 (2004), 2965.
- [10] ETACHERI V., ROSHAN R., VISWANATHAN K., *ACS Appl. Mater. Inter.*, 4 (2012), 2717.
- [11] WOAN K., PYRGIOTAKIS G., SIGMUND W., *Adv. Mater.*, 21 (2009), 2233.
- [12] CHEN C.S., XIE X.D., CAO S.Y., LIU T.G., CHEN X.H., LIU Q.C., MEI Y.P., ZHAO G.J., *Funct. Mater. Lett.*, 6 (2013), 1350018.
- [13] ZHANG Z.H., *Phys. Rev. B*, 66 (2002), 085405.
- [14] KONGKANAND A., DOMYNGUEZ R.M., KAMAT P.V., *Nano Lett.*, 7 (2007), 676.
- [15] KONGKANAND A., KAMAT P.V., *ACS Nano*, 1 (2007), 13.
- [16] LEARY R., WESTWOOD A., *Carbon*, 49 (2011), 741.
- [17] JIANG L.Q., GAO L., *Mater. Chem. Phys.*, 91 (2005), 313.
- [18] ZHU L.P., LIAO G.H., HUANG W.Y., MA L.L., YANG Y., YU Y., FU S.Y., *Mater. Sci. Eng. B-Adv.*, 163 (2009), 194.
- [19] KHATAEE A.R., ZAREI M., *Desalination*, 278 (2011), 117.
- [20] CHEN C.S., LIU T.G., LIN L.W., XIE X.D., CHEN X.H., LIU Q.C., LIANG B., YU W.W., QIU C.Y., *J. Nanopart. Res.*, 15 (2013), 1295.
- [21] SALEH T.A., GONDAL M.A., DRMOSH Q.A., YAMANI Z.H., AL-YAMANI A., *Chem. Eng. J.*, 166 (2011), 407.
- [22] CHEN X.H., CHEN C.S., CHEN Q., *Mater. Lett.*, 57 (2002), 734.
- [23] CHEN C.S., XIE X.D., LIU T.G., LIN L.W., KUANG J.C., XIE X.L., LU L.J., CAO S.Y., *J. Nanopart. Res.*, 14 (2012), 817.
- [24] KIM T.H., PARK J.J., NAM S.H., PARK H.S., CHEONG N.R., SONG J.K., PARK S.M., *Appl. Surf. Sci.*, 255 (2009), 5264.
- [25] LU X.Y., LIU Z.Y., ZHU Y., JIANG L., *Mater. Res. Bull.*, 46 (2011), 1638.
- [26] AKSOY S., CAGLAR Y., ILICAN S., CAGLAR M., *J. Alloy. Compd.*, 512 (2012), 171.
- [27] PETRELLA A., PETRELLA M., BOGHETICH G., MASTRORILLI P., PETRUZZELLI V., RANIERI E., PETRUZZELLI D., *Ind. Eng. Chem. Res.*, 52 (2013), 2201.
- [28] BACHILO S.M., STRANO M.S., KITRELL C., *Science*, 298 (2002), 2361.
- [29] VANHEUSDEN K., WARREN W.L., SEAGER C.H., TALLANT D.R., VOIGT J.A., *J. Appl. Phys.*, 79 (1996), 7983.
- [30] DAS S., CHAKRABARTI S., CHAUDHURI S., *J. Phys. D Appl. Phys.*, 38 (2005), 4021.
- [31] KIM D.T., YU K.S., KIM W.T., KIM C.D., PARK H.L., *J. Mater. Sci. Lett.*, 11 (1992), 886.
- [32] FANG D.Y., LI C.L., WANG N., LI P., YAO P., *Cryst. Res. Technol.*, 48 (2013), 265.
- [33] YANG X.L., XU G.F., LI H.P., ZHU J.G., WANG X., *Cryst. Res. Technol.*, 31 (1996), 521.
- [34] FUJIHARA S., OGAWA Y., KASAI A., *Chem. Mater.*, 16 (2004), 2965.
- [35] SUWANBOON S., AMORNPIKOSUK P., *Proc. Eng.*, 32 (2012), 821.

Received 2013-05-31

Accepted 2015-05-19